Surface structure of protonated R-sapphire ($1\bar{1}02$) studied by Sum-Frequency Vibrational Spectroscopy

Jaeho Sung,† Luning Zhang,† Chuanshan Tian,† Glenn A. Waychunas,‡ and Y. Ron Shen*,†

†*Department of Physics, University of California, Berkeley, California 94720, and*

‡*Earth Sciences Division, Lawrence Berkeley National Laboratory, Berkeley, California 94720*

Email:yrshen@calmail.berkeley.edu

Abstract

Sum frequency vibrational spectroscopy was used to study the protonated R-plane ($1\bar{1}02$) sapphire surface. The OH stretch vibrational spectra show that the surface is terminated with three hydroxyl moieties, two from $AlOH_2$ and one from Al_2OH functional groups. The observed polarization dependence allows determination of the orientations of the three OH species. The results suggest that the protonated sapphire ($1\bar{1}02$) surface differs from an ideal stoichimetric termination in a manner consistent with previous X-ray surface diffraction (crystal truncation rod) studies. However, in order to best explain the observed hydrogen-bonding arrangement, surface oxygen spacing determined from the X-ray diffraction study requires modification.

Introduction

Surfaces and interfaces of metal oxides have been the subject of intensive investigation in recent years because they play an important role in many natural and technological processes, including mineral dissolution, adsorption/desorption reactions, soil and aquifer toxic and nutrient transfer, heterogeneous catalysis, and corrosion/weathering.[1-9] To understand these processes, the zeroth-order knowledge required the static molecular surface structure, or termination surface, of the oxides in contact with aqueous solution. This is not easily obtainable due to limitations of the available surface probe techniques. Electron probes are exclusively restricted to ultrahigh vacuum or special differentially-pumped systems, and hence can provide

information only on dry and often specially cleaned surfaces (e.g. LEED, XPS). X-ray probes are commonly used for both surface spectroscopy and surface diffraction, and have been limited to vacuum surfaces in the past. [10-14] However over the last decade or so, surface diffraction has been extended to solid/water interfaces with good success. [15-19] Nevertheless, such scattering studies remain limited, as they cannot directly measure low atomic number species such as H, and generally provide information only on the most ordered aspects of interface structure. Recently, surface specific sum-frequency vibrational spectroscopy (SFVS) has been added to the arsenal of tools to study metal oxide surfaces and interfaces.[20-24] SFVS has the capability of probing surfaces exposed to air as well as interfaces buried under liquids and solids. Moreover, the surface vibrational spectrum is directly related to the surface structure of a material, is highly sensitive to structural variations involving protons, and is able to sample different interfacial species. Thus, SFVS appears to be an excellent complement to the other methods in the prevailing arsenal. In this paper, we report our recent study of the sapphire R-plane ($1\bar{1}02$) surface using SFVS and compare our findings with previous x-ray scattering and simulation results. The R-plane surface is one of the stable termination facets on natural corundum (and hematite) crystals, and is known to be a highly active surface for anion sorption. Hence it has been the subject of several recent studies on mineral surface reactivity and contaminant uptake. [25-28]

Sapphire (α-Al_2O_3), also known as the mineral corundum, is one of the most common and technologically important metal oxides. It is isostructural with hematite (α-Fe_2O_3), which is another important metal oxide for both modern science and technology, and in environmental sciences. Surface investigations of α-Al_2O_3 have been mainly focused on the high symmetry (0001) (C-plane) surface.[14-15, 29-31] An X-ray diffraction (crystal truncation rod, or CTR) study found that the α-Al_2O_3 (0001) surface structure in equilibrium with a water layer in air is terminated with a near bulk stoichiometry topology, but with relaxation in interlayer distances as predicted by calculations.[15] The fully protonated surface was predicted to be dominated by Al_2OH functional groups, and this was later confirmed by SFVS.[21] For the α-Al_2O_3 ($1\bar{1}02$) surface, three general structures have been proposed (Fig. 1). A CTR study concluded that the deprotonated surface was terminated by three distinct kinds of relaxed oxygen layers bonded to 3Al, 2Al, and 1Al, respectively, (Fig. 1a) deviating from the

ideal stoichimetric bulk termination (Fig. 1b).[16] (The relaxed bulk termination model to well fit CTR data in Ref. 16 appears to have unreasonable Al-O bond lengths.) The results of a CTR study on isostructural α-Fe_2O_3 also found the same three kinds of oxygen layers on the $(1\bar{1}02)$ surface,[17] Both cases were consistent with a "missing layer" of Al or Fe beneath the uppermost oxygen layer, when compared to the stoichiometric termination. The α-Fe_2O_3 $(1\bar{1}02)$ surface was also examined by DFT simulations, which predicted three hydroxyls, two associated with $FeOH_2$ and one from Fe_2OH, on the surface, in agreement with a bond-valence interpretation of the CTR results.[32] Thus, given that fully protonated α-$Fe_2O_3(1\bar{1}02)$ could be (although not necessarily) isostructural with fully protonated α-Al_2O_3 $(1\bar{1}02)$ surface, the presence of three types of OH, two from $AlOH_2$ and one from Al_2OH, are also expected. There is a recent X-ray reflectivity study on an hydrated α-Al_2O_3 $(1\bar{1}02)$ surface.[33] The results suggested a fully terminated surface structure having singly and triply Al-coordinated surface oxygens that can be protonated (Fig. 1c). Assuming the structures of air/α-Al_2O_3 $(1\bar{1}02)$ and water/α-Al_2O_3 $(1\bar{1}02)$ interfaces are the same, (although this is not necessarily true), we can also expect three types of OH with this termination, two from $AlOH_2$ and one from Al_3OH, A recent DFT calculation, comparing the free energies of different surface structures of α-Al_2O_3 $(1\bar{1}02)$ under various conditions, found that this type of surface termination (Fig. 1c) was the most stable at room temperature in UHV , but under ambient pressure the CTR missing layer structure (Fig. 1a) model is more stable, being only 1.8 meV/Å lower in energy.[34]

For a better understanding of the surface structure of α-Al_2O_3 $(1\bar{1}02)$, one would like to resort to additional surface probe techniques. We note that X-ray probes are generally not sensitive to protons, and therefore cannot provide much information on protons adsorbed at surfaces, except indirectly as deduced from observed bond length variations and known bond length systematics. Thus there is no direct observation of how the α-Al_2O_3 $(1\bar{1}02)$ surface is protonated. In this paper, we present a study on protonated α-Al_2O_3 $(1\bar{1}02)$ in air using SFVS as a probe, which is known to be sensitive to different surface OH species. The spectra enable us to identify the different types of hydroxyls on the surface and their orientations, from which we can deduce a reasonable surface structure for the protonated α-Al_2O_3 $(1\bar{1}02)$.The results show that there are three different

types of hydroxyls on the surface as predicted by the CTR missing-layer model and the fully terminated model from X-ray reflectivity. However, the stretch frequencies and orientations of the these hydroxyls are not consistent with the latter, leaving the missing-layer structure as the only plausible one for the α-Al_2O_3 ($1\bar{1}02$) surface we have investigated. This surface structure can serve as a base for future investigation of how the Al_2O_3 ($1\bar{1}02$) surface reacts in aqueous solutions to pH changes and surface complexation.

Theoretical background

The basic theory of SFVS for surface studies has been described elsewhere.[35-37] Here, we present only the key points needed for data analysis. The SF signal generated by overlapping incoming beams of frequencies ω_{vis} and ω_{ir} at a surface in the reflected direction is given by

$$I(\omega) = \frac{8\pi^3\omega^2 \sec^2\beta}{c^3} |\chi_{eff}^{(2)}|^2 I_1(\omega_{vis}) I_2(\omega_{ir}) \qquad (1)$$

where I_i is the light intensity at frequency ω_i and β is the reflection angle of the SF output. The effective surface nonlinear susceptibility has the expression,

$$\vec{\vec{\chi}}_{eff}^{(2)} = [\hat{e}(\omega_{SF}) \cdot \vec{\vec{L}}(\omega_{SF})] : \vec{\vec{\chi}}^{(2)} \cdot [\hat{e}(\omega_{vis}) \cdot \vec{\vec{L}}(\omega_{vis})][\hat{e}(\omega_{IR}) \cdot \vec{\vec{L}}(\omega_{IR})] \qquad (2)$$

with $\hat{e}(\omega_i)$ being the unit polarization vector and $\vec{\vec{L}}(\omega_i)$ the transmission Fresnel factor of light of frequency ω_i at the interface. The surface nonlinear susceptibility $\vec{\vec{\chi}}^{(2)}$ can be approximated by

$$\overleftrightarrow{\chi}^{(2)} = \overleftrightarrow{\chi}_{NR}^{(2)} + \sum_q \frac{\vec{\vec{A}}_q}{(\omega_{IR} - \omega_q) + i\Gamma_q}, \qquad (3)$$

with the nonresonant contribution denoted by $\overleftrightarrow{\chi}_{NR}^{(2)}$, and the resonant contribution assumed to come from discrete vibrational resonances with resonant frequencies ω_q and damping constants Γ_q. The resonance amplitude $\vec{\vec{A}}_q$ is defined as

$$\begin{aligned} \vec{\vec{A}}_q &= \int \vec{\vec{a}}_q(\Omega) f(\Omega) d\Omega \\ &\equiv N_q < \vec{\vec{a}}_q > \end{aligned} \qquad (4)$$

where $\vec{a}_q$ is the resonant amplitude of the qth mode from an individual molecule, and N_q and $f(\Omega)$ are the surface density and the orientation distribution function of the molecules contributing to the qth mode. The tensor elements of $\vec{\vec{A}}_q$ in the lab coordinates (i,j,k) are related to those of $\vec{a}_q$ in the molecular coordinates (ξ,η,ζ) by

$$A_{q,ijk} = N_q \sum_{\xi,\eta,\zeta} <(\hat{i}\cdot\hat{\xi})(\hat{j}\cdot\hat{\eta})(\hat{k}\cdot\hat{\zeta})> a_{q,\xi\eta\zeta} \qquad (5)$$

It is possible to determine the parameters characterizing the resonances by fitting the measured $|\chi^{(2)}_{eff}|^2$ spectrum with proper input/output polarization combinations using Eqs. (1-3). However, the fitting may not be unique unless the resonant frequencies and the signs of $\vec{\vec{A}}_q$ are pre-chosen. The latter often requires a phase measurement on the SF output such that the Im $\chi^{(2)}$ spectrum can be obtained to directly characterize the resonances.[36-40] For discrete resonances, Im $\chi^{(2)}$ has the expression

$$\mathrm{Im}\,\vec{\vec{\chi}}^{(2)} = \sum_q \frac{\vec{\vec{A}}_q \Gamma_q}{(\omega_{IR}-\omega_q)^2+\Gamma_q^2} \qquad (6)$$

Experimental

We measured SF vibrational spectra of the air/sapphire ($1\bar{1}02$) interface in the OH stretch region. Our SFVS setup has been described elsewhere. [39, 40] Briefly, we overlapped two input beams, one fixed at visible wavelength 532 nm and the other tunable in the infrared between 2.6 and 3.7μm, with typical energies of ~500 μJ/pulse and ~100 μJ/pulse, respectively, in a spot of 180x300 μm^2 on the sample surface. The pulses had a width of ~20 ps and were incident on the sample at angles of $\beta_{vis}=45^o$ and $\beta_{IR}=57^o$ from the air side. We detected the SF signal in the reflection direction, which was spatially and spectrally filtered and then collected by a gated detector system. Each data point was obtained from averaging over 200 laser shots, and was normalized against that from a z-cut quartz plate. We also carried out phase measurement of SFVS using the interference scheme described in Ref. [41, 42].

The sample used was an epi-polished single crystal of α-Al_2O_3 ($1\bar{1}02$) purchased from Princeton Scientific Corporation. The sample was 5 mm thick, and the root-mean-square roughness of the polished surfaces measured by atomic force microscopy (AFM) was less than 0.1 nm. (see Supporting Information for the AFM image) Sample preparation followed the recipe of Ref. [15, 43, 44]. The sample surface was first cleaned in a sonication bath of acetone, methanol, and pure water for 10, 10, and 60min, respectively, in sequence. It was then mildly etched in a 10~15mM solution of HNO_3 under sonication for 30min, rinsed thoroughly with deionized water, and blow-dried by filtered nitrogen gas. To remove the remaining water and organic contaminates on the surface, the sample was heated at ~350^{o}C for 1 hour. After cooling down to room temperature in nitrogen atmosphere, the sample was mounted in a sealed Teflon cell for measurement.

Result & Discussion

In the experiment, we first made sure that the cleaned sample surface had all unwanted adsorbates removed. We compare in Fig. 2 the SSP (denoting S-, S-, P-polarized SF output, visible and infrared inputs, respectively) SF vibrational spectra of the air/α-Al_2O_3($1\bar{1}02$) interface before and after the sample was baked at ~350^{o}C for 1 hour. The spectrum before baking exhibits residual signal in the CH stretch region from organic contaminants on the surface, and the spectrum after baking does not. The spectrum in the O-H stretch region decreases but displays more pronounced features after baking, suggesting that physically adsorbed water molecules had also been removed. The AFM image of the baked sample shows that the surface was crystalline to the unit cell level. The spectrum was not observed to change, even after remaining 24 hours in a nitrogen-filled cell, but if it was left in air for ~24 hours, the spectrum would return to that before baking. We discuss here SF spectroscopic results on the baked sample.

Shown in Fig. 3 are the SF vibrational spectra of the sapphire ($1\bar{1}02$) surface after heating with three different input/output polarization combinations: SSP, SPS, and SSS. All spectra can be fitted using Eqs. (1-3) with three discrete resonant modes having resonant frequencies (ω_q) at 3365, 3520, and 3670 cm^{-1}, respective

bandwidths (Γ_q) of 70, 90, and 120 cm^{-1}, and amplitudes (A_q) of positive sign that corresponds to O→H pointing to the vapor side. The sign of A_q was determined by making phase measurements at several frequencies of the SF output.[39, 45] As shown in Fig. 4, the positive A_q led to all positive SSP $\mathrm{Im}\,\overleftrightarrow{\chi}^{(2)}$ spectra for all three different azimuthal orientations. We plot in Figs. 3 and 4 the three individual resonant modes deduced from fitting of the spectra. The appearance of these modes allows us to check which surface structural model for α-Al_2O_3 ($1\bar{1}02$) is reasonable.

We consider first the three models of α-Al_2O_3 ($1\bar{1}02$) described in the introduction section. The ideal bulk-terminated model (Fig. 1b) has the surface oxygen bonded to three underlying Al atoms. It appears unlikely that H would bind on Al_3O to form Al_3OH if we evaluate this oxygen's bond valence (to be described below). Even if this bonding did occur, the single surface OH species is not consistent with observation of three OH stretch modes in the SFVS spectra of Fig. 3. Therefore, the ideal bulk-terminated model must be ruled out. The model (Fig. 1c) proposed by the X-ray reflectivity study [33] is also found to be inconsistent with our sample surface as it would have only two different OH species from $AlOH_2$ while adsorption of H to form Al_3OH would remain unlikely, again from the bond valence argument. Even if protonation of Al_3O were possible, it could not explain the observed spectrum. As we shall discuss later, the 3670 and 3520 cm^{-1} modes should be assigned to stretch vibrations of the dangling and H-bonded OHs of $AlOH_2$ at the surface, leaving the 3365 cm^{-1} mode possibly assigned to Al_3OH. Since 3365 cm^{-1} is significantly red-shifted from the dangling OH frequency, [46, 47] the H of Al_3OH would have to be H-bonded to a neighboring O at the surface, but no such O can be found in the proposed structure of Ref. 33. One may want to assign the 3670 and 3365 cm^{-1} modes to $AlOH_2$ and the 3520 cm^{-1} mode to Al_3OH, but the orientation of OH deduced from our spectral results (presented later) does not agree with this model. Moreover, a recent study on how the spectrum of the water/α-Al_2O_3 ($1\bar{1}02$) interface changes with pH in water clearly supports the assignment of the 3520cm^{-1} mode to the H-bonded OH of $AlOH_2$.[48] The CTR model [16] (Fig. 1a) (equivalent to the bulk-terminated model with the top layer of Al atoms removed), on the other hand, does suggest the presence of three different OH

species, from $AlOH_2$ and Al_2OH, at the protonated surface.

As mentioned in Sec. 1 and sketched in Fig. 1a, the CTR model for α-Al_2O_3 $(1\bar{1}02)$ shows three different surface oxygen species with equal numbers bonded to 1Al, 2Al, and 3Al, respectively.[16] The proton affinity of these terminating oxygens can be estimated by their bond valence values. The latter can be deduced from the CTR result, and permit assignment of possible hydroxyl species on the surface. Oxygen in the topmost layer is bonded to a single Al, and has a bond valence of 0.3.[16] The ideal sum of all bond valences on an oxygen should equal to its valence state of 2, and hence this oxygen is clearly underbonded.[49, 50] A proton on average adds 0.8 bond valence unit to its oxygen if it forms an additional hydrogen bond, and 1.0 bond valence unit otherwise. Hence the oxygen of AlO can have two protons bound to it, one of which would be expected to be dangling (not forming other hydrogen bonds) and the other H-bonded with a neighboring O. Oxygen in the second layer is bonded to two Al atoms and has a bond valence of 1.2,[16] which still allows one proton chemically bound to it but also hydrogen-bonded to another neighboring O. Finally, oxygen in the third layer with bonding to three Al atoms has a bond valence of 1.6,[16] and is not likely to be protonated, although it is still possible to receive a proton via hydrogen bonding, i.e. act as a hydrogen bond acceptor, with a neighboring hydroxyl. These bond valence values for oxygen at the α-Al_2O_3 $(1\bar{1}02)$ surface are very similar to those at the α–Fe_2O_3 $(1\bar{1}02)$ surface. The latter has bond valence values of 0.3, 1.1 and 1.6, respectively, for the three surface oxygen species.[17, 32] Thus, the three OH stretch modes observed in our SF spectra can be identified with the three OH species on the protonated α-Al_2O_3 $(1\bar{1}02)$ surface, two from $AlOH_2$ and one from Al_2OH. Based on their frequencies, the 3670 cm^{-1} mode can be identified with the dangling OH on $AlOH_2$ and the 3520 cm^{-1} and 3365 cm^{-1} modes with the H-bonded OH groups of $AlOH_2$ and Al_2OH. We assign the 3520 cm^{-1} mode to OH of $AlOH_2$ H-bonded to the oxygen of a neighboring $AlOH_2$, and the 3365 cm^{-1} mode to OH of Al_2OH H-bonded to the oxygen of a neighboring Al_3O group.

To confirm the above assignment, we need to obtain the orientations of the three OH species and show that they agree with those predicted from the appropriate surface structural model of the α–Al_2O_3 $(1\bar{1}02)$. The OH orientations can be deduced from the polarization dependence of the OH stretch modes in the SF spectra.

According to the CTR (or bulk-terminated) model in Fig. 1a, the surface structure of α–$Al_2O_3(1\bar{1}02)$ has a $(\bar{1}\,\bar{1}20)$ glide plane, hence hydroxyls on the oxygen chains along this glide plane exiting the surface form pairs consistent with the glide symmetry. Since the glide plane yields the same symmetry relations for surface optical nonlinearity as a mirror plane, the α–$Al_2O_3(1\bar{1}02)$ surface should exhibit C_{1v} structural symmetry in SFVS. Figure 3 shows the measured SSP, SPS, and SSS spectra for γ = 0, 90° and 180°, where γ is the azimuthal angle between the incidence plane and the direction $[1\,\bar{1}0\,\bar{1}]$ in the glide plane $(\bar{1}\,\bar{1}20)$. Using Eqs. (1-3) to fit the spectra, we can deduce the strength A_q of the three OH modes in each spectrum. We have measured the SSP spectra for a number of different γ, and the deduced $A_q(\mathrm{SSP})$ versus γ is plotted in Fig. 5, showing that the strengths exhibit C_{1v} structural symmetry. From Figs. 3-5, and knowing that effective excitation of an OH stretch mode requires an IR input with a polarization component along the OH bond, we obtain the following qualitative information on the orientations of the OH species on α–$Al_2O_3(1\bar{1}02)$. For the dangling O-H pairs contributing to the mode at 3670 cm^{-1}, the weaker SPS signal compared to SSP at all γ implies that the OH's incline more toward the surface normal, and the forward/backward asymmetry in the plot of Fig. 5c indicates that they have a forward tilt. (The forward direction is denoted by $[1\,\bar{1}0\,\bar{1}]$). For the mode at 3520 cm^{-1}, the relatively strong SPS signal suggests the corresponding OH's are tilted significantly away from the surface normal, and the forward-backward asymmetry in Fig. 5b indicates that the OH's have a backward tilt. For the mode at 3365 cm^{-1}, the weak SSP signal and the plot in Fig. 5a suggests that the OH's incline more toward the surface and away from the glide plane with a slight forward tilt.

Quantitative analysis of the OH spectra, following the procedure described in the literature,[51-53] yields quantitative information on the orientations of the OH species. (See Supporting Information for more details.) As we mentioned earlier, fitting the SF spectra with Eqs. (1)-(3) allows us to determine $(A_q)(\hat{e}_{SF}, \hat{e}_{vis}, \hat{e}_{ir}; \gamma)$, with $\hat{e}_i$ denoting the polarization of the ω_i wave. Figure 5 displays $(A_q)(SSP;\gamma)$ versus γ for the three OH stretch modes. Equation (5) can then be used to find the orientations of the three OH species specified by the polar angle θ_0 with respect to the surface normal and the azimuthal angle ϕ_0 with respect to the forward

direction along the glide plane. (See Fig. 6), assuming the orientational distribution function in Eq.(4) is a δ-function in θ_0 and ϕ_0. The fit also yields the polarizability ratio $\alpha^{(2)}_{q,\eta\eta\xi}/\alpha^{(2)}_{q,\xi\xi\xi}$ for the OH bond, where $\alpha^{(2)}_{q,\xi\xi\xi}$ and $\alpha^{(2)}_{q,\eta\eta\xi}=\alpha^{(2)}_{q,\zeta\zeta\xi}$ are the nonvanishing elements of the SF polarizability tensor of the qth OH stretch mode with ξ denoting direction along the OH bond and η and ζ perpendicular to the bond. We find θ_0 =36°±9°, ϕ_0 =±78°±9°, and $\alpha^{(2)}_{\eta\eta\xi}/\alpha^{(2)}_{\xi\xi\xi}$ =0.32±0.04 for the 3670cm^{-1} mode, θ_0 =62°±8°, ϕ_0 =±127°±9°, and $\alpha^{(2)}_{\eta\eta\xi}/\alpha^{(2)}_{\xi\xi\xi}$=0.38±0.03 for the 3520cm^{-1} mode, and θ_0=69°±12°, ϕ_0=±67°±10°, and $\alpha^{(2)}_{\eta\eta\xi}/\alpha^{(2)}_{\xi\xi\xi}$=0.37±0.06 for the 3365cm^{-1} mode.

We expect that the proper protonated surface structure of α-Al_2O_3 ($1\bar{1}02$) must show the existence of three surface OH species with their orientations close to the ones described above. The criteria for a proper surface structure are: first, it must be periodic in the surface plane, and second, the H-bonding strength of the bonded OH species must be reasonably strong. The latter requires that OH---O has an approximate triangular arrangement, with a bending angle OH---O sufficiently large (>150°), and with O---H distance appropriate (between 1.5 and 2.1 Å).[54-56] Additionally, for significant H-bonding, the angle between O---H and the axis of the lone-pair (LP) orbital of O should be less than the angular half-width of the lone-pair orbital (~38°). [57, 58] We show below that under such criteria, the missing-layer surface structure (Fig. 1a) of α-Al_2O_3 ($1\bar{1}02$) derived from the CTR model,[16] although qualitatively correct with the proper C_{1v} symmetry, still needs modification in its structural dimensions,

We first focus on the $AlOH_2$ groups. In Fig. 7, we show two neighboring rows of O in the top surface layer of the CTR model structure[16] along the direction of the glide plane. The H's adsorbed on O's in the form of $AlOH_2$ are projected on the surface plane in the figure. We assume tetrahedral bonding geometry for O. The azimuthal orientations of the projected LP of O, the H-bonded OH, and the dangling OH on the surface plane are specified by α, β, and δ with respect to the O—O lines, respectively, as labeled in Fig. 7. For a given separation ρ between the two oxygen rows, if either α, β, or δ is specified, the orientations of two hydroxyls

of $AlOH_2$ are completely determined from the required condition that the structure is periodic. If we take the OH bond length to be 0.95 Å and the angle between two neighboring tetrahedral bonds to be109.5°,[58, 59] we can find, for given ρ and α (or β or δ), the bent angle κ of OH---O, the H---O distance d, and the angular deviation ψ of the oxygen LP orbital from O---H (κ, d and ψ are described in the inset of Fig. 7). As we mentioned earlier, significant H-bonding of O---H must satisfy the condition $\kappa > \sim 150^{\circ}$, $\psi < \sim 38^{\circ}$, and d ~ 1.5 to 2.1 Å. Therefore, for a given ρ, we can vary α and calculate κ, ψ, and d to see the range of α the condition of significant H-bonding for H of $AlOH_2$ to be bonded to the neighboring O. We first test out the CTR missing-layer model structure with ρ = 0.29 Å.[16] We find that the maximum κ appears at $\kappa_{max} \sim 156^{\circ}$ with corresponding $\psi \sim 63^{\circ}$ and d ~1.68 Å, or the minimum ψ appears at $\psi_{min} \sim 30^{\circ}$, with corresponding $\kappa \sim 126^{\circ}$ and d ~ 2.08 Å. Neither set of geometric parameters, nor any other sets, with the given ρ value satisfies the requirement for significant H-bonding. Thus the CTR model with ρ = 0.29 Å[16] is inconsistent with the observed H-bonded OH mode associated with $AlOH_2$. In view of the fact that the CTR model has oxygen rows shifted from their bulk termination positions, we can consider a modified CTR model with a different ρ value.

In Fig. 8(a), we show the calculated κ_{max} and the corresponding ψ and d as functions of ρ. There are no references in the literature that allow us to directly evaluate the H-bonding strength with given κ, ψ and d. However, a recent simulation study provides, for given κ and d, the H-bonding probability, $P(\kappa,d)$, obtained after integration over all values of ψ.[55, 56] We know that H-bonding probability, $P(\kappa,d,\psi)$, should decrease with increase of ψ from zero, and simply assume that it is proportional to $\exp[-\psi^2/\sigma^2]$, where σ is the half width of the oxygen LP orbital. We can then plot in the same frame of Fig. 8a the relative H-bonding probability, $P(\kappa,d,\psi) = P(\kappa_{max}, d)\exp[-\psi^2/\sigma^2]$, of OH---O versus ρ. The maximum H-bonding probability appears at ρ = 1.1 Å with $\kappa_{max} = \sim 165^{\circ}$, $\psi = \sim 25^{\circ}$ and d = 1.89 Å. The corresponding orientations of the H-bonded OH and the dangling OH are found to be ($\theta_{0B} \sim 85^{\circ}$, $\phi_{0B} \sim \pm 155^{\circ}$) and ($\theta_{0D} \sim 50^{\circ}$, $\phi_{0D} \sim \pm 80^{\circ}$), respectively, in rough agreement with the experimentally deduced orientations given before ($\theta_{0B} \sim 62^{\circ}$, $\phi_{0B} \sim \pm 127^{\circ}$ and $\theta_{0D} \sim 36^{\circ}$, $\phi_{0D} \sim \pm 78^{\circ}$). If we use the empirical rule of Rozenberg et al (valid for $\kappa > 150^{\circ}$) to

estimate the red shift of H-bonded OH from the dangling OH, $\log(\Delta\nu / cm^{-1}) = -1.97 - 6.1\log(\mathrm{d}/nm)$,[59] we obtain $\Delta\nu \sim 285\pm50\mathrm{cm}^{-1}$, which is in fair agreement with the observed $\Delta\nu \sim 200\mathrm{cm}^{-1}$, considering that the rule may have overestimated the shift for κ appreciably different from 180°. We note that this optimized ρ value of 1.1 Å is closer to the value of 0.95 Å in the bulk structure and considerably larger than the value of 0.29 Å from the CTR model[16].

We can also emphasize instead the importance of minimizing ψ for H-bonding. In doing this, we obtain, from a similar geometric calculation, ψ_{min} and the corresponding κ and d as well as the H-bonding probability versus ρ, shown in Fig. 8b. The maximum H-bonding probability appears again at ρ = 1.1 Å with corresponding $\psi_{min} = \sim15^{o}$, κ = ~155° and d = 1.91 Å. Note that this set of values for ρ, ψ, κ and d is not far from that of the previous case despite the emphasis on minimizing ψ instead of maximizing κ. In the present case, for the maximum H-bonding probability, the orientations of the H-bonded OH and the dangling OH are found to be ($\theta_{0B} \sim 80^{o}$, $\phi_{0B} \sim \pm150^{o}$) and ($\theta_{0D} \sim 45^{o}$, $\phi_{0D} \sim \pm85^{o}$), respectively, and the red shift of the bonded OH to be $\Delta\nu \sim 275\pm50\mathrm{cm}^{-1}$, again in rough agreement with the experimental result.

The bonded OH mode at 3365 cm^{-1} associated with Al_2OH also cannot be explained by the CTR model. We need to adjust the separation between the second and third oxygen surface layers. We follow the same approach described above. In this case, if the layer separation h between the second and third surface layers is fixed, the orientations for the OH's (specified by θ_0 and ϕ_0) are completely determined, and the set of values for κ, d, and ψ can be calculated. We plot, in Fig. 9, κ, ψ, and d as well as the H-bonding probability as a function of h. The maximum H-bonding probability appears at h ~ 0.35 Å, with κ ~ 155°, d ~ 1.7 Å, and ψ ~ 20°. The corresponding orientation of the bonded OH is specified by $\theta_0 \sim 85^{o}$ and $\phi_0 \sim \pm60^{o}$, and the red-shift of the bonded OH frequency is estimated to be ~ 630±110 cm^{-1} (which again, compared to the observed $\Delta\nu \sim 400\ \mathrm{cm}^{-1}$, is probably overestimated because of the appreciable difference of κ from 180°) The layer spacing, h, deduced here is ~0.55 Å less than that of the bulk structure and ~0.3 Å smaller than that of the CTR model[16].

The discrepancy in the surface structural parameters deduced by us and by the CTR work [16] may come

from different sample preparation procedures. For the CTR measurement, the sample was first mildly etched in 0.01M HNO_3 solution, followed by multiple rinses with Milli-Q water and heating to ~350°C in air. After the sample was cooled down to room temperature, it was extensively washed with Milli-Q water and blown dry by an Ar jet. It was then annealed at ~900°C for 1 hour in $1x10^{-6}$ Torr O_2 followed by Ar ion sputtering for 30 min. Afterwards, the sample was further annealed at ~750 °C in $2x10^{-6}$ Torr O_2 for 1 hour and at ~1000 °C for 1 hour. The CTR measurements were then carried out on the sample in UHV after it was dosed with water. Increasing water gas pressure from $1x10^{-8}$ to 1.6 Torr was used for dosing, but no difference was found in the CTR result. Comparing the sample preparation procedure described above with the one we used, one may suspect that the high-temperature annealing and Ar ion sputtering could have stabilized the surface structure of α–Al_2O_3 $(1\bar{1}02)$ so that it was not easily protonated with water dosing. An earlier study had indicated that the α-Al_2O_3 (0001) surface may not be fully hydrated under water pressure <1 Torr.[60] It is thus possible that the sample surface measured in the CTR work is in some way structurally different from ours.

Conclusion

We have used SFVS to study the protonated surface structure of α-Al_2O_3 $(1\bar{1}02)$ in air by probing the OH stretch vibrational modes at the surface. The spectra exhibit C_{1v} symmetry expected from the crystalline bulk structure. Three distinct OH species are detected: one dangling OH and two H-bonded. Their orientations, deduced from spectral dependences on input/output polarizations and sample orientation, allow us to check which of several possible surface structure models is reasonable. We find that the presence of three OH species cannot be explained by either the bulk-terminated model, or the model of Catalano et al. deduced from X-ray reflectivity measurements, but can be explained by the model of Trainer et al. deduced from the CTR measurement. The three OH stretch peaks in the spectra can be assigned to a dangling OH and an H-bonded OH associated with $AlOH_2$ of the topmost oxygen layer and another H-bonded OH associated with the Al_2OH of the second oxygen surface layer. However, we determined that the oxygen spacing of the surface structure described in the CTR model does not permit surface hydroxyls with appreciable hydrogen bonding, and

requires modification to be consistent with our other results. By varying the oxygen row separation along the glide plane and the layer separation at the surface in the CTR model, we obtain a surface structure where the H-bonded hydroxyl groups have optimum H-bonding strength. In this modified surface structure of protonated α-Al_2O_3 ($1\bar{1}02$), the orientations and the estimated stretch frequencies of the three OH species are all in rough agreement with the experimental findings from SFVS.

Our study shows that SFVS can provide complementary information to X-ray measurements of the surface structures of metal oxides and lead to a more complete characterization of such surfaces. It also sets up a useful basis for further investigation of water/metal oxide interface structures, which are important in many disciplines. As the next step in extending this approach, we are in the process of studying aqueous-solution/α-Al_2O_3 ($1\bar{1}02$) interfaces using different pH conditions. By comparing both the dry and fully wet-equilibrated surfaces, we expect to obtain a molecular-structure explanation consistent with the observed interfacial acid-base properties.

Acknowledgement

The authors thank Prof. Young-Shin Jun (Washington Univ, St. Louis) and Dr. David Singer (UC Berkeley/LBNL) for help with AFM analysis, and several anonymous reviewers for helpful comments which significantly improved the final manuscript. This work was supported by the Director, Office of Science, Office of Basic Energy Sciences, Chemical Sciences, Geosciences, and Biosciences Division of the U.S. Department of Energy under contract No. DE-AC02-05CH11231, and by the NSF Science and Technology Center of Advanced Materials for Purification of Water with Systems (Water CAMPWS; CTS-0120978).

Supporting Information Available: Sample AFM image analysis and fitting parameters of SFVS spectra. This information is available free of charge via Internet at http://pubs.acs.org.

References

(1) Stumm, W.; Morgan, J. J., Aquatic Chemistry: Chemical Equilibria and Rates in Natural Waters, third ed., Wiley Interscience, New York, 1996.

(2) Cornell, R. M.; Schwertmann, U., Iron Oxides: Structure, Properties, Reactions, Occurrence, and Uses, first ed., Wiley-VCH, 1996.

(3) Weiss, W.; Ranke, W., *Prog. Surf. Sci.* **2002,** 70, 1.

(4) Apostolescu, N.; Geiger, B.; Hizbullah, K.; Jan, M.T.; Kureti, S.; Reichert, D.; Schott, F.; Weisweiler W., *Appl. Catal. B: Environ.* **2006**, 62, 104.

(5) Lee, E.; Jung, K.; Joo, O.; Shul, Y., *Appl. Catal. A: Gen.* **2005**, 284, 1.

(6) Zheng, Y.; Cheng, Y.; Wang, Y.; Bao, F.; Zhou, L.; Wei, X.; Zhang, Y.; Zheng, Q., *J. Phys. Chem. B* **2006**, 110, 3093.

(7) A. Kuch, *Corros. Sci.* **1998**, 28, 221.

(8) Kouloumbi, N.; Tsangaris, G. M.; Vourvahi, C.; Molnar, F., *J. Coat. Technol.* **1997**, 69, 53.

(9) Ernst, M.; Lurot, F.; Schrotter, J.-C., *Applied Catalysis B: Environmental*, **2004**, 15

(10) Gautier-Soyer, M.; Pollak, M.; Henriot, M.; Guittet, M. J., *Surf. Sci.* **1996**, 352–354, 112

(11) Lad, R. J.; Henrich, V. E., *Surf. Sci.* **1988**, 193, 81.

(12) Henderson, M. A. *Surf. Sci.* **1994**, 319, 315.

(13) Henderson, M. A.; Joyce, S. A.; Rustad, J. R., *Surf. Sci.* **1998**, 417, 66.

(14) Guenard, P.; Renaud, G.; Barbier, A.; Gautier-Soyer, M. *Surf. Rev. Lett.* **1998**, 5, 321.

(15) Eng, P. J.; Trainor, T. P.; Brown Jr., G. E.; Waychunas, G. A.; Newville, M.; Sutton, S. R.; Rivers, M. L., S*cience* **2000**, 288, 1029.

(16) Trainor, T. P.; Eng, P. J.; Brown Jr., G. E.; Robinson, I. K.; De Santis, M., *Surf. Sci.* **2002**, 496, 238.

(17) Tanwar, K. S.; Lo, C. S.; Eng, P. J.; Catalano, J. G.; Walko, D. E.; Brown Jr., G. E.; Waychunas, G. A.; Chaka, A. M.; Trainor, T. P., Surf. Sci. **2007**, 601, 460.

(18) Fenter, P.A.; Cheng, L.; Park, C.; Zhang, Z.; Sturchio, N.C. *Geochim. Cosmochim. Acta* **2003**, 67, 4267.

(19) Fenter, P.A., *Rev. Mineral. Geochem*. **2002**, 49, 149.

(20) Yeganeh, M. S.; Dougal, S. M.; Pink, H. S. *Phys. Re*v. *Lett.* **1999**,*83*, 1179.

(21) Zhang, L.; Tian, C. S.; Waychunas, G. A.; Shen, Y. R., *J. Am. Chem. Soc.* **2008**, 130, 7686.

(22) Chandrasekharan, R.; Zhang, L.; Ostroverkhov, V.; Prakash, S.; Wu, Y.; Shen, Y. R.; Shannon, M. A., *Surf. Sci.* **2008**, 602, 1466.

(23) Braunschweig, G., Eissner, S., and Daum, W. *J. Phys. Chem. C* **2008,** 112, 1751.

(24) Mathias, F.; Klaus, K.; Robert, P.; Ahmed, A.; Bernd, S; Reinhardt, K.; Thomas, F. *Langmuir* **2008**, 24, 13434.

(25) Bargar, J. R.; Towle, S. N.; Brown Jr., G. E.; Parks, G. A. *Geochim. Cosmochim. Acta* **1996**, 60, 3541.

(26) Templeton, A. S.; Trainor, T. P.; Traina, S. J., Spormann, A. M.; Brown Jr., G.E. *Proc. Natl. Acad. Sci. USA* **2001**, 98, 11897.

(27) Trainor, T. P.; Templeton, A. S.; Brown Jr., G. E.; Parks, G. A. *Langmuir* **2002**, 18, 5787.

(28) Catalano, J. G.; Trainor, T. P.; Eng, P. J.; Waychunas, G. A.; Brown Jr., G. E. *Geochim. Cosmochim. Acta*

2005, 69, 3555.
(29) Ahn, J.; Rabalais, J. W., *Surf. Sci.* **1997**, 388, 121.
(30) Wang, X. G.; Chaka, A.; Scheffler, M., *Phys. Rev. Lett.* **2000**, 84, 3650.
(31) Hass, K. G.; Schneider, W. F.; Curioni, A.; Andreoni, W. *J. Phys. Chem. B* **2000**, 104, 5527.
(32) Lo, C. S.; Tanwar, K. S.; Chaka, A. M.; Trainor, T. P., *Phys. Rev. B* 2007, 75, 075425.
(33) Catalano J. G.; Park G.; Zhang Z.; Fenter P.; Langmuir **2006**, 22, 4668.
(34) Mason S. E.; Iceman, C. R.; Trainor, T. P; Chaka, A. M., *Phys. Rev. B* 2010, 81, 125423
(35) Shen, Y. R., *Annu. Rev. Phys. Chem.* **1989**, 40, 327 .
(36) Shen, Y. R., *Surf. Sci.* **1994**, 299/300, 551 .
(37) Miranda, P. B.; Shen, Y. R., *J. Phys. Chem. B* **1999**, *103*, 3292.
(38) Ji, N.; Ostroverkhov, V.; Chen, C.-Y.; Shen, Y. R. *J. Am. Chem. Soc* **2007**, *129*, 10056.
(39) Tian, C. S.; Ji, N.; Waychunas, G. A.; Shen, Y. R., *J. Am. Chem. Soc* **2008**, 130, 13033.
(40) Zhang L.; Seema S.;Tian, C.; Shen Y. R.; Wu Y.; Shanon M. A.; Brinker C. J., *J. Chem. Phys.* **2009**, 130, 154702.
(41) Ostroverkhov, V.; Waychunas, G. A.; Shen, Y. R. *Chem. Phys. Lett.* **2004**, 386, 144–148.
(42) Ostroverkhov, V.; Waychunas, G. A.; Shen, Y. R. *Phys. Rev. Lett.* **2008**, 94, 046102.
(43) Franks, G. V.; Meagher, L. *Colloids Surf., A* **2003**, *214*, 99–110.
(44) Fitts, J. P.; Shang, X. M.; Flynn, G. W.; Heinz, T. F.; Eisenthal, K. B. *J. Phys. Chem. B* **2005**, *109*, 7981–7986.
(45) Ji, N.; Ostroverkhov V.; Tian, C. S.; Shen, Y. R. *Phys. Rev. Lett.***2005**, 100, 096102.
(46) Busca, G.; Lorenzelli, V.; Escribano, V. S.; Guidetti, R. *J. Catal.***1991**, 131, 167.
(47) Morterra, C.; Magnacca, G. *Catalysis Today* **1996**, 27, 497.
(48) Sung, J.; Zhang, L.; Tian, C. S.; Waychunas, G. A.; Shen, Y. R. (to be published).
(49) Bickmore, B. R.; Rosso, K. M.; Tadiner, C. J.; Bylaska E. J.; Daud, D. *Geochim. Cosmochim. Acta* **2006,** 70, 4057.
(50) Brown, I. D., The Chemical Bond in Inorganic Chemistry: The Bond Valence Model. Oxford Press, New York, 2002.
(51) Wei, X.; Zhuang, X.; Hong, S. C.; Goto, T.; Shen, Y. R., *Phys. Rev. Lett.* **1999**, 82, 4256
(52) Oh-e, M.; Kim, D.; Shen, Y. R., *J. Chem. Phys.* **2001**, 115, 5582.
(53) Kim, D.; Oh-e, M.; Shen, Y. R. *Macromolecules* **2001**, 34, 9125.
(54) Mezei, M.; Beveridge, D. L. *J. Chem. Phys.* **1981**, 74, 622.
(55) Kumar, R.; Schmidt, J. R.; Skinner, J. L. *J. Chem. Phys.* **2007**, 126, 204107.
(56) Auer, B. M.; Skinner, J. L. *Chem. Phys. Lett.* **2009**, 470, 13.
(57) Ducan, A. B. F.; Pople, J. A. *Trans. Faraday Soc.* **1953**, 49, 217.
(58) Eisenberg, D.; Kauzmann, W., The structure and Properties of the Water, Oxford Press, New York, 2005.
(59) Rozenberg, M.; Loewenschuss, A.; Marcus, Y. *Phys. Chem. Chem. Phys.* **2002**, 2, 2699.
(60) Liu, P.; Kendelewicz, T.; Brown, G. E., Jr.; Nelson, E. J.; Chambers, S. A. *Surf. Sci.* **1998**, *417*, 53.

Figure captions

Figure 1. Surface structures of α-$Al_2O_3(1\bar{1}02)$ obtained from (a) CTR measurement, (Side and top views of the structure are displayed on the left and right, respectively. The surface is terminated by equal numbers of singly (AlO, Green), doubly (Al_2O, Purple) and triply (Al_3O, Yellow) coordinated oxygen atoms.) (b) ideal bulk stoichimetric termination, and (c) X-ray reflectivity measurement. Red and blue spheres represent oxygen and aluminum, respectively.

Figure 2. SSP spectra obtained in the following conditions : before (green triangle) and after (black triangle) heating the sample at 350°C for ~1 hour, after keeping the sample in the cell for ~24 hours (blue triangle) and exposing to the air for ~24 hours at the outside of the cell (red triangle) , respectively.

Figure 3. SFVS spectra of protonated α-$Al_2O_3(1\bar{1}02)$ surface with input/output polarization combinations (a) SSP, (b) SPS and (c) SSS. Spectra for different sample orientations specified by γ (defined as shown in (d)) are displayed separately in different frames. Solid black lines are fits obtained using Eq. (5), and blue, purple and red lines describe the discrete resonant components at 3365, 3520 and 3670 cm^{-1} deduced from fitting.

Figure 4. Im $\chi^{(2)}$ spectra deduced from the corresponding SSP-$|\chi^{(2)}|^2$ spectra at γ ~0, 90 and 180° in Fig. 3a, where blue, purple and red lines describe the discrete resonant components at 3365, 3520 and 3670 cm^{-1} deduced from fitting. The crosses indicate the points where values of Im $\chi^{(2)}$ have been confirmed by SFVS phase measurement.

Figure 5. Resonant amplitude versus azimuthal orientation of the sample for the three OH modes in the SSP spectra: (a) 3365, (b) 3520 and (c) 3670cm^{-1}. The polar angle in the plots refers to the angle between the incidence plane and the glide symmetry plane of the sample. Lines are fit to the data points.

Figure 6. Schematic showing the geometric relation between the molecular coordinates (ξ,ζ,η) attached to an O-H group and the laboratory coordinates (X,Y,Z), where X and Y are the same directions with $[1\bar{1}0\bar{1}]$ and $[\bar{1}\bar{1}20]$, respectively. The large and small spheres represent oxygen and hydrogen, respectively.

Figure 7. Schematic describing two neighboring rows of O in the topmost layer of α-$Al_2O_3(1\bar{1}02)$ and the projection of H's on the oxygen plane. Circles represent oxygen, and LP denotes lone-pair orbital of O. The inset shows the parameters that are used to define hydrogen bonding of O---H.

Figure 8. (a) κ_{max} and the corresponding ψ and d versus oxygen row spacing ρ as well as H-bonding probability, $P(\kappa_{max}, \psi, d)$, versus ρ. (b) ψ_{min} and the corresponding k and d versus ρ as well as H-bonding probability, $P(\kappa, \psi_{min}, d)$, versus ρ.

Figure 9. ψ, κ, and d versus layer separation h, as well as H-bonding probability as varying layer separation $P(\kappa, \psi, d)$ versus ρ.

Figure 10. Surface structures deduced from the CTR and SFVS result combined with the hydrogen bonding optimization showing (a) side and (b)top views of fully protonated α-$Al_2O_3(1\bar{1}02)$ surface.

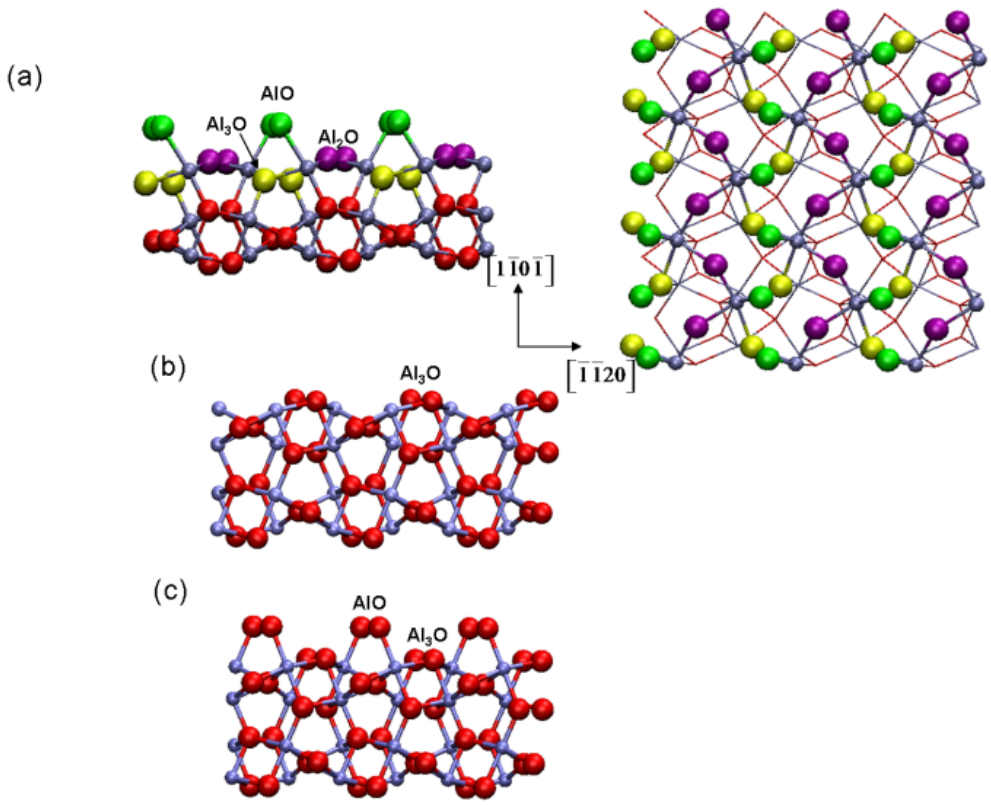

Figure 1.

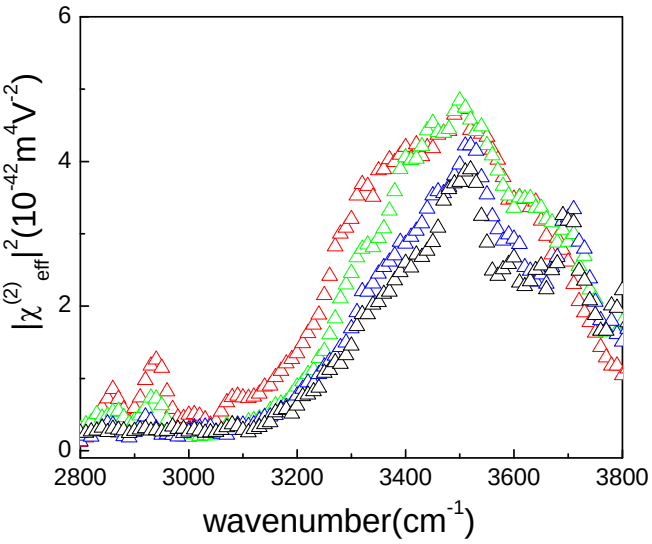
6
4
2
0
2800
3000
3200
3400
3600
3800
wavenumber(cm-1)
|χ(2)eff|2(10-42m4V-2)

Figure 2.

Figure 3.

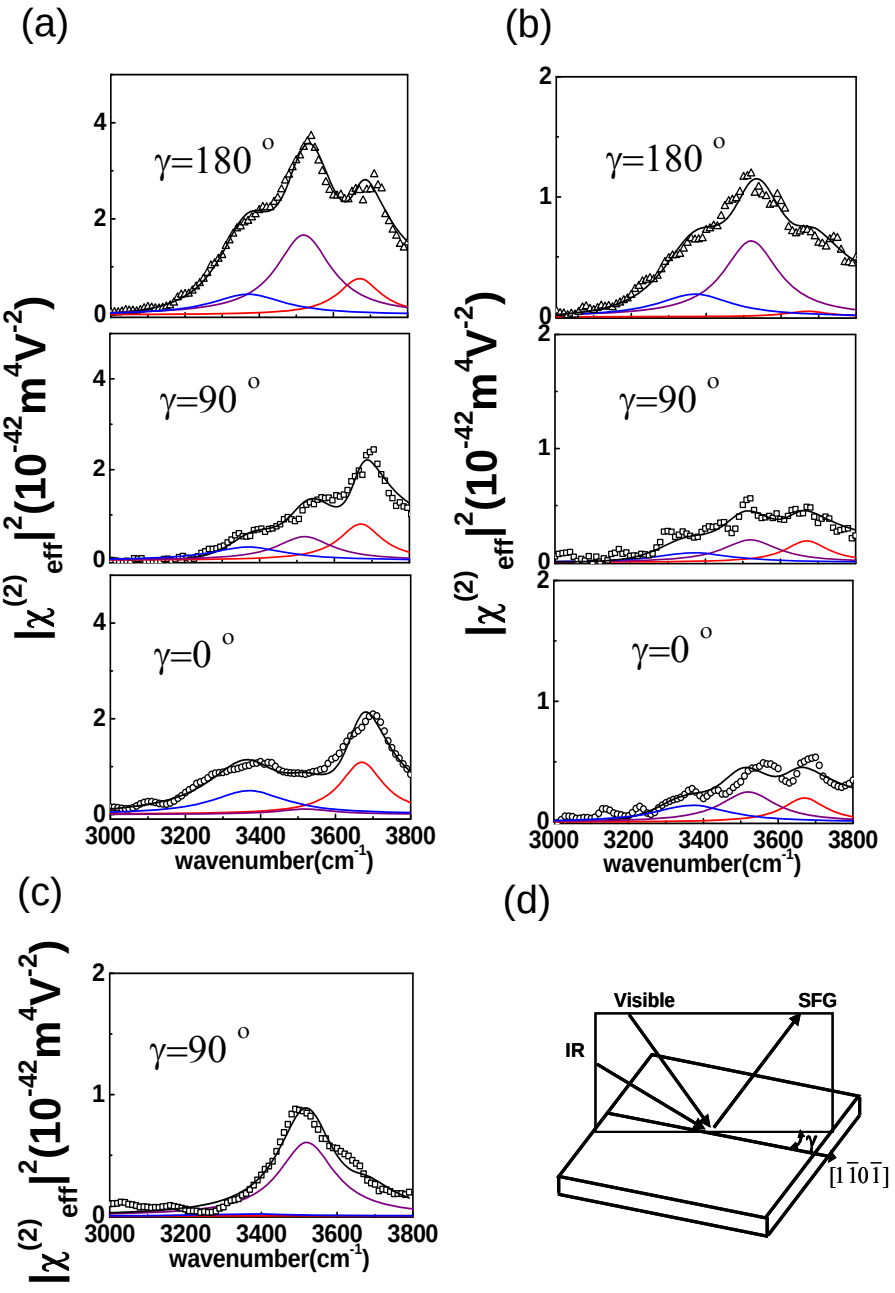

Figure. 3

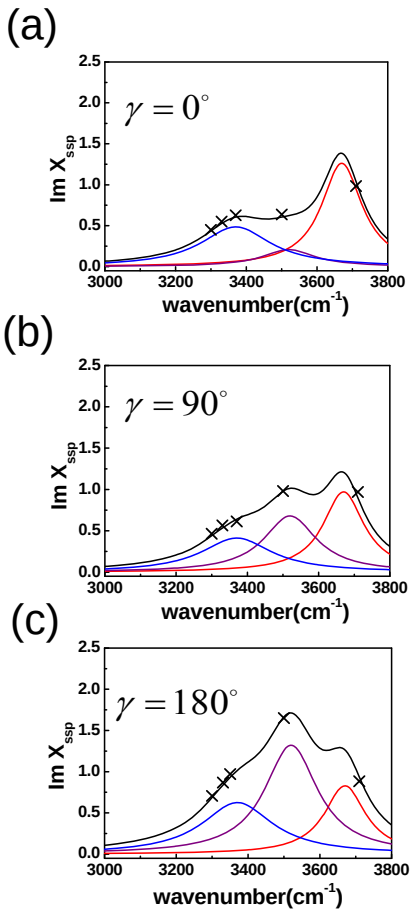
(a)
$\gamma = 0^\circ$
Im X_{ssp}
wavenumber(cm^{-1})
(b)
$\gamma = 90^\circ$
Im X_{ssp}
wavenumber(cm^{-1})
(c)
$\gamma = 180^\circ$
Im X_{ssp}
wavenumber(cm^{-1})

Figure 4.

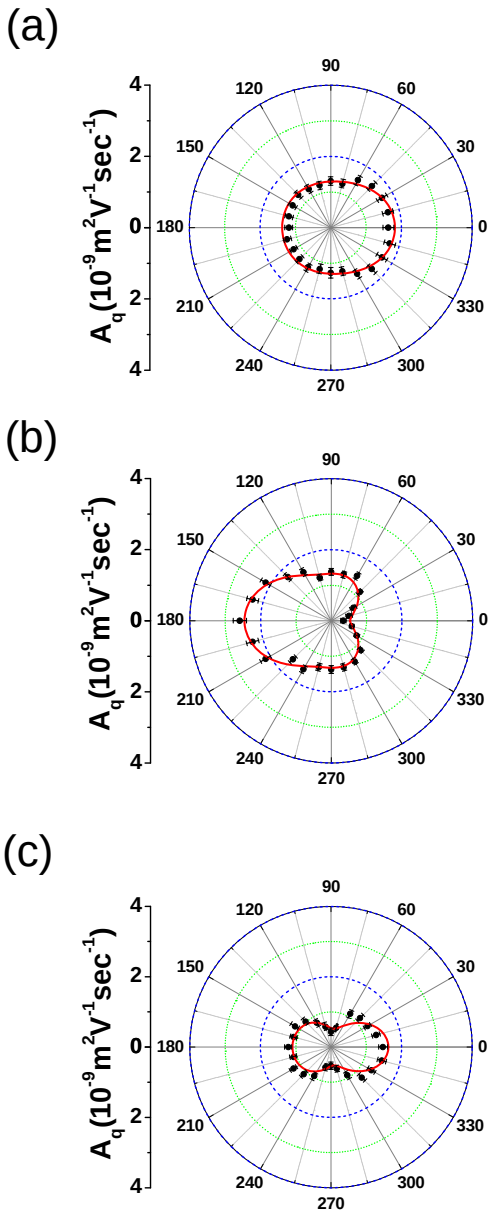
(a)
(b)
(c)
$A_q(10^{-9}m^2V^{-1}sec^{-1})$
90
120
60
150
30
180
0
210
330
240
300
270
4
2
0
2
4

Figure 5.

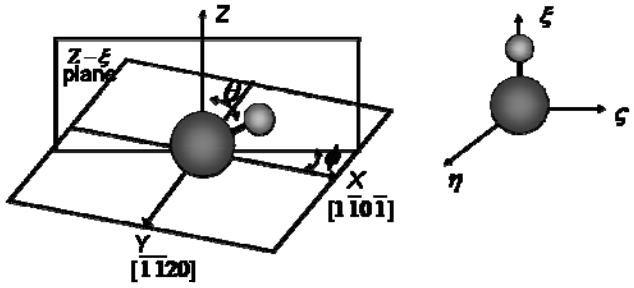

Figure 6.

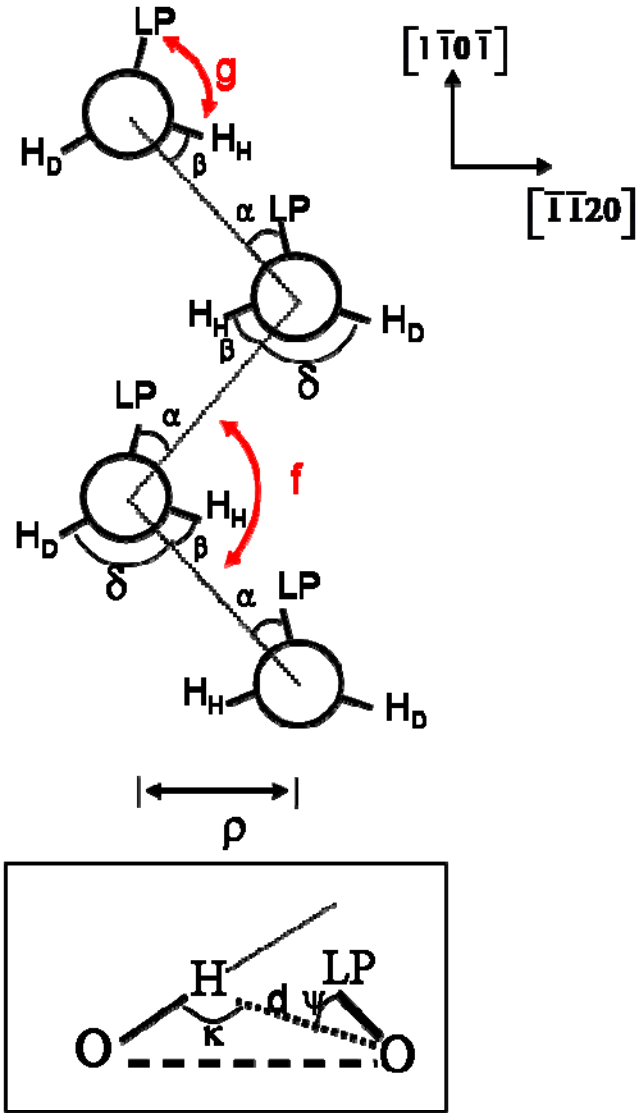
LP
g
H_D
H_H
β
α LP
H_H
β
H_D
δ
LP
α
f
H_H
H_D
β
δ
α LP
H_H
H_D
ρ
[1 1̄ 0 1̄]
[1̄ 1̄ 2 0]
H
LP
d
ψ
κ
O
O

Figure 7.

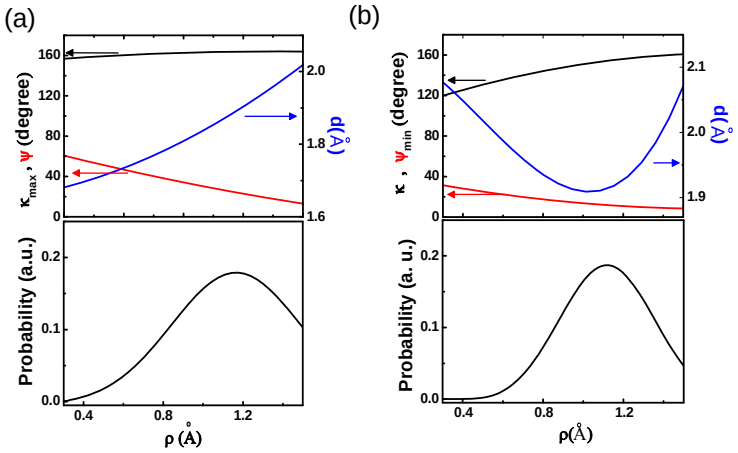
(a)
(b)
160
120
80
40
0
2.0
1.8
1.6
d(Å)
Probability (a.u.)
0.2
0.1
0.0
0.4
0.8
1.2
ρ (Å)
2.1
1.9
ρ(Å)

Figure 8.

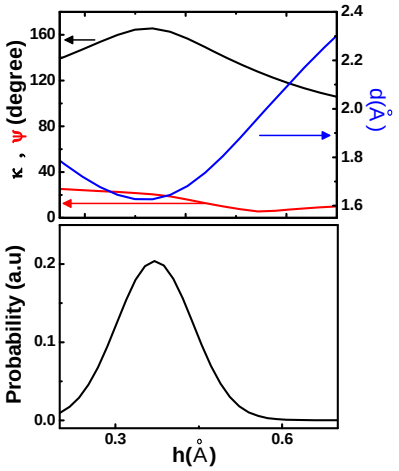
160
120
80
40
0
κ , ψ (degree)
2.4
2.2
2.0
1.8
1.6
d(Å)
0.2
0.1
0.0
Probability (a.u)
0.3
0.6
h(Å)

Figure 9.

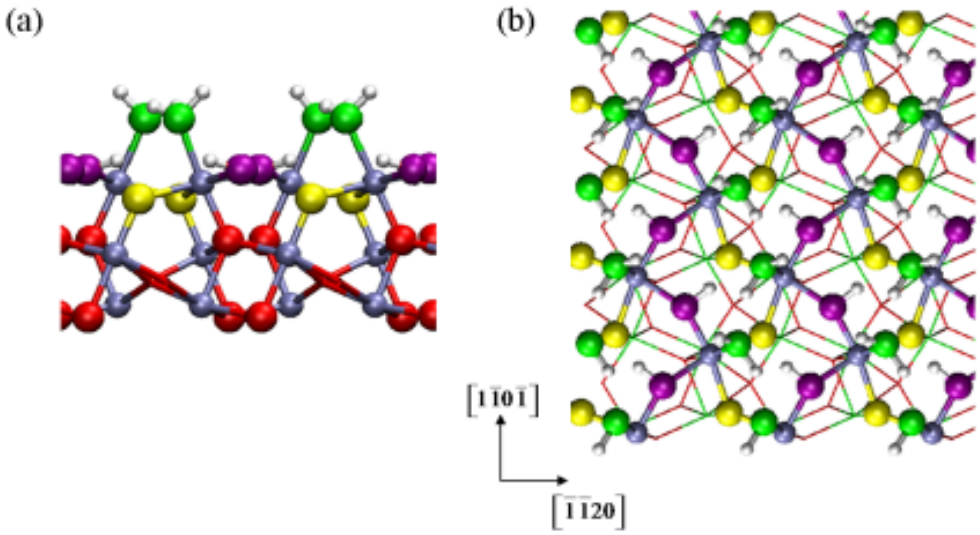

Figure. 10